ACS APPLIED MATERIALS & INTERFACES

Research Article

Cite This: ACS Appl. Mater. Interfaces 2018, 10, 3241−3247

www.acsami.org

Artificial NO and Light Cooperative Nanofluidic Diode Inspired by Stomatal Closure of Guard Cells

Ruirui Li, Xin Sui, Chao Li, Jiaqiao Jiang, Jin Zhai,* and Longcheng Gao*

Key Laboratory of Bio-Inspired Smart Interfacial Science and Technology of Ministry of Education, School of Chemistry, Beihang University, Beijing 100191, P. R. China

Supporting Information

ABSTRACT: Gas messenger molecule (NO) plays important roles in K^+ nanochannels of guard cells by binding directly to the heme-containing enzymes. Inspired by this natural phenomenon, we developed artificial K^+ nanochannels modified with ferroporphyrin, where NO triggered the nanochannels to turn "ON" states from the ferroporphyrin blocked "OFF" states. The mechanism relies on the fact that NO has higher affinity with ferroporphyrin compared to carboxyl groups on the nanochannel surface. The synergistic effect of the released carboxyl groups and the conically asymmetric shape leads the ion transportation to be diode-like. However, the nanofluidic diode properties vanished after illumination with light to remove NO from the ferroporphyrin−NO complex. This NO and light cooperative nanofluidic diode possesses excellent stability and reversibility, which shows great promise for use in gas detection and remote control of mass delivery.

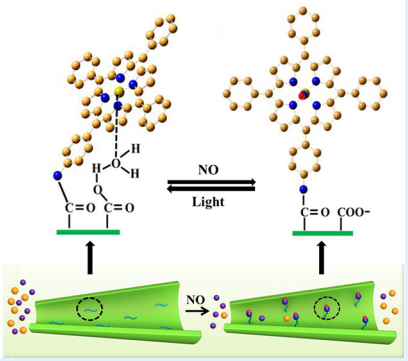

KEYWORDS: *NO, light, nanofluidic diode, ion transport, gas detection, mass delivery*

1. INTRODUCTION

Nitric oxide (NO), a highly reactive free radical, exists in all living cells.[1−3] In plants, NO can be produced from nitrate reductase reduction of nitrite.[4] NO functions as a versatile signal molecule in the physiology of plants, such as plant development, programmed cell death, and so forth.[5,6] It can interfere with signal cascade and regulate diverse ion flux in channels[7−10] through the coordination to heme-containing enzymes. For example, NO triggers stomatal closure of guard cells to reduce transpiration of plants.[11−13] Heme binds to guanylate cyclase, inhibiting its catalytic activity (Figure 1a). As NO is endogenously generated, NO coordinates to the heme center, releasing the guanylate cyclase, another signal molecule cyclic guanosine monophosphate (cGMP) was subsequently generated. These signals regulate Ca^{2+}-sensitive K^+ channels at the plasma membrane to facilitate solute efflux, resulting in the stomatal closure and inhibiting the transpiration of plants.[14] In this way, plants can enhance tolerance to drought, avoiding droop in drought.

Inspired by the NO-regulated ion channels in nature, building robust artificial ion channels activated by NO in vitro is significantly important, avoiding the instability and fragility of biological ion channels in an external environment.[15−17] NO-regulated ion channels have great potential applications, such as actuators and nanofluidic diodes. To date, artificial ion channels that can respond to external stimuli, such as pH,[18−21] light,[22−25] temperature,[26−28] biomolecules,[29,30] specific ions,[31,32] electric field,[33,34] and mechanical stress[35] have been extensively reported. However, the artificial nanochannels that respond to signal gases, especially NO, have been seldom reported, because the NO triggered systems are always composed of multistep and synergistic procedures.[36] However, the complicated and delicate physiological processes in which NO is involved play significant roles in the activities of life. Therefore, the design and construction of biomimetic NO-regulated nanochannels with applications in nonliving systems is in high demand.

Ferroporphyrin is an essential moiety of many enzymes and proteins.[37] The highly reactive NO molecule attacks the ferrous center of ferroporphyrin forming the nitrosyl adducts, and the nitrosyl adducts can lose NO after exposure to visible light.[38] Herein, we designed an NO and light cooperative nanofluidic diode by modifying ferroporphyrin onto conical nanochannels in porous polyethylene terephthalate (PET) membrane. Like the ion channels in nature, the key factor lies in establishing a dynamic coordination system.[11] As NO is highly reactive, it preferentially coordinates to ferroporphyrin, altering the interaction between ferroporphyrin and the carboxyl groups attached on nanochannels (Figure 1b). In particular, ferroporphyrin was modified onto the nanochannels. The ferroporphyrin coordinated to the residual carboxyl groups, making the nanochannels more hydrophobic (Figure S1 of the Supporting Information, SI). The surface of nanochannels become close-to-neutral state, and the ion transport was inhibited. NO was used as a trigger to release the carboxyl groups, due to its higher affinity with ferroporphyrin. The

Received: September 24, 2017
Accepted: January 5, 2018
Published: January 5, 2018

DOI: 10.1021/acsami.7b14505
ACS Appl. Mater. Interfaces 2018, 10, 3241−3247

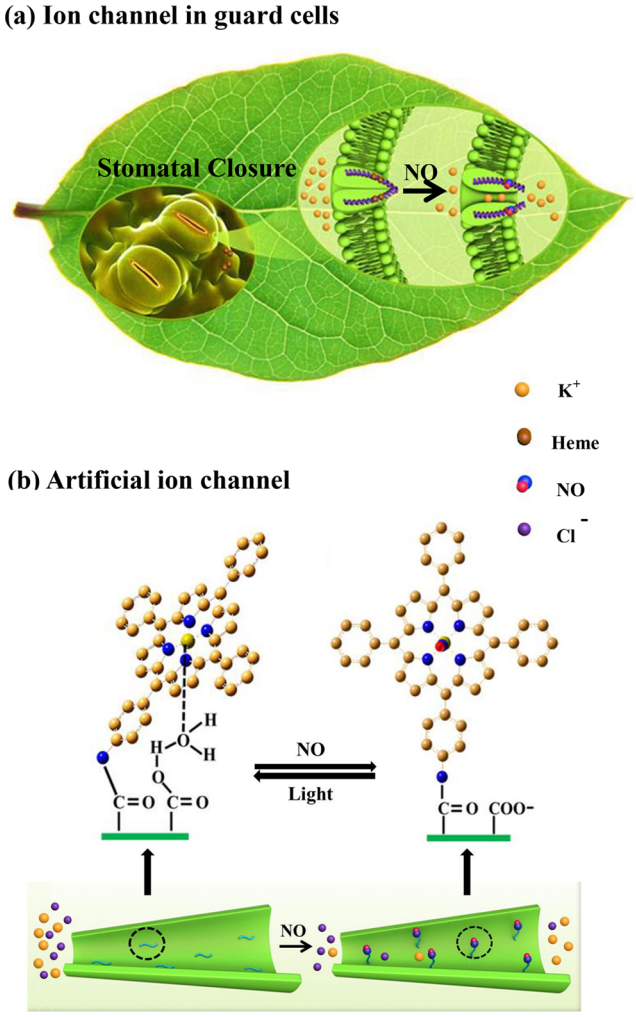

Figure 1. (a) NO-activated ion channels in guard cells. NO generated in guard cells can promptly coordinate to heme of the guanylate cyclase, releasing the inhibitory effect of the heme. Thus, the guanylate cyclase can be activated, and hence regulate the Ca^{2+}-sensitive K^+ channels. (b) Artificial NO-activated ion channel. Ferroporphyrin molecules were grafted onto the inner surface of the conical-shaped nanochannels, leading to an OFF-state. NO binds to ferroporphyrin, releasing the carboxyl acid on the nanochannel surface. The channel surface becomes negatively charged, resulting in the ON-state. After illumination with light, the carboxyl acid coordinated to ferroporphyrin and the surface became neutral, and the gate turned to the OFF-state.

cooperation between the released carboxyl groups and asymmetric shape enabled the nanochannels to rectify the ion current. Interestingly, the nanofluidic sensing system is reversible. The coordination reaction (Figure S2) we introduced in this system can be regulated by light. After light exposure, NO dissociated from the ferroporphyrin−NO complex. Thus, ferroporphyrin coordinated to the carboxyl groups again. The nanochannels recovered OFF-states. The switching between ON- and OFF-states of the nanochannels can repeat several cycles. Therefore, an NO and light cooperative nanofluidic diode was realized with excellent reversibility and stability, which shows great potential applications in the fields of actuators and remote control of mass delivery.

2. EXPERIMENTAL SECTION

2.1. Nanochannels Fabrication. The nanochannels were prepared based on our previous work.[39] In a typical experiment, PET films (23 μm thick) were irradiated with an Au-ion beam to form multiple cylindrical pores (5×10^8 cm^{-2} track density). Conical nanochannels were obtained through ion-track etching technique. Before etching, the membranes were irradiated under UV light (365 nm) for 2 h from both sides. Then, the ion track polymer membrane was chemically etched at a stationary temperature (about 50 °C) with etching solution (9 M NaOH) on one side, and stopping solution (1 mol L^{-1} KCl and 1 mol L^{-1} HCOOH) on the other side of membrane to neutralize the etchant as soon as the pore opened (Figure S3). After the etching process, the residual salts were removed by washing with Milli-Q water (18.2 MΩ) several times. The size of the large opening was about 450 nm detected by scanning electron microscopy (Figure S4).

2.2. Chemical Modification. The carboxyl (—COOH) groups were generated on the channel surface during the ion track-etching process. Amino ferroporphyrin was modified onto the inner surface of the nanochannels through coupled reaction. First, the carboxyl groups were activated into amine-reactive esters by means of carbodiimide coupling chemistry. Then, these reactive esters were further combined with amino groups of ferroporphyrin through the formation of covalent bonds. For the activation of carboxyl groups, the PET film was exposed to 1-ethyl-3-(3-dimethyla minopropyl) carbodiimide hydrochloride (100 mmol L^{-1}) in ethanol solution for 1 h. After washing with deoxygenated water several times, the PET films were transferred into a culture dish containing amino ferroporphyrin (10 mmol L^{-1}) for 4 h at room temperature. Since NO is highly reactive, all the reaction equipment and solutions involved should be purged with N_2 for 30 min before bubbling NO.

2.3. Preparation of Amino Ferroporphyrin. The amino ferroporphyrin was obtained from precursor amino porphyrin, which was synthesized by sequential nitration and reduction of tetraphe-

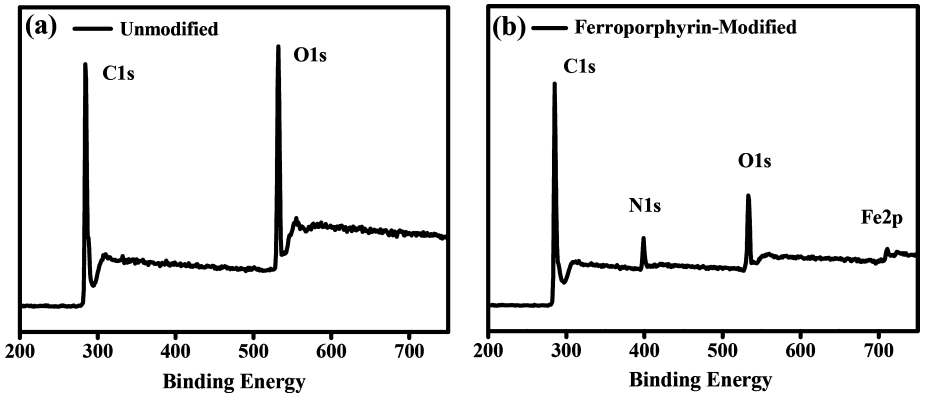

Figure 2. XPS spectrum of PET films before (a) and after (b) ferroporphyrin modification.

DOI: 10.1021/acsami.7b14505
ACS Appl. Mater. Interfaces 2018, 10, 3241−3247

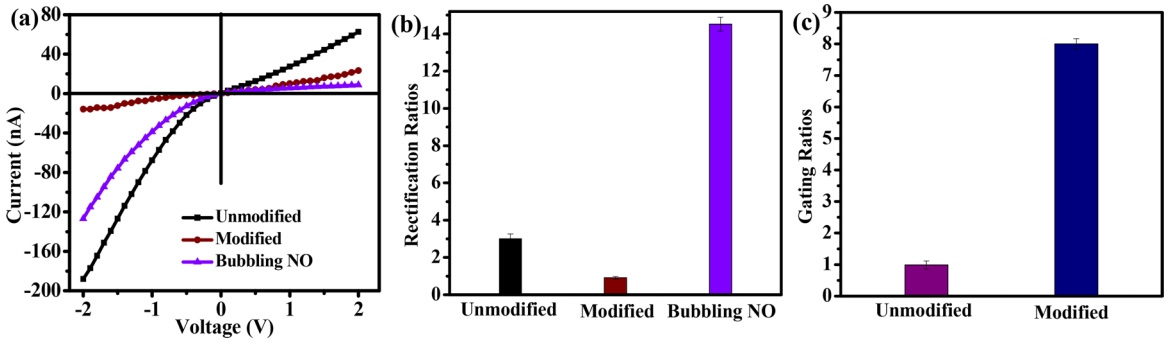

Figure 3. (a) Current−voltage (I−V) curves of the porous nanochannels in 0.1 M KCl electrolyte solution: before ferroporphyrin modification (black line), after ferroporphyrin modification (wine line), and the modified nanochannels after bubbling NO (violet line). (b) The corresponding rectification ratios of the unmodified (black column), modified (wine column) nanochannels and the modified nanochannels after bubbling NO (violet column). (c) Gating ratios of the modified and unmodified nanochennals which were calculated by the ion current measured in the presence and absence of NO at −2 V.

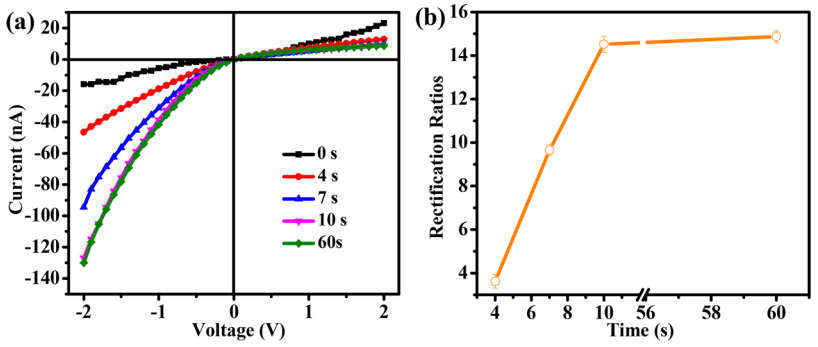

Figure 4. (a) The transmembrane *I*−*V* curves with different NO ventilation time. (b) The rectification ratio variation under different NO ventilation time.

nylporphyrin. The aminoporphyrin and $FeCl_2$ were refluxed in *N*,*N*-dimethylformamide (DMF) for 2 d under nitrogen atmosphere. Finally, amino ferroporphyrin was attained from column separation.

2.4. Current−Voltage Measurement. The ionic current through unmodified and modified channels was measured by a Keithley 6487 picoammeter (Keithley Instruments, Cleveland, OH). A porous conical PET nanochannel membrane was mounted between two chambers of the etching cell (Figure S5). Potassium chloride (Beijing Chemical Factory) aqueous solutions with different concentrations at pH 7 were chosen as electrolyte. The membrane was bubbled with NO in ethanol before current measurement. NO flow rate is 8 mL s^{-1}. The scanning voltage varied from −2 to +2 V; Ag/AgCl electrodes were used to measure the resulting ion current.

3. RESULTS AND DISCUSSION

Ferroporphyrin was immobilized onto the inner surface of the nanochannels by one step coupling reaction between amino ferroporphyrin and carboxyl acid. The modification was certified by X-ray photoelectron spectroscopy (Figure 2). Before modification, only C 1s and O 1s signals can be detected. After modification, obvious peaks assigned to N 1s and Fe 2p appeared, demonstrating the successful modification.

The transmembrane ion current through nanochannels was mearured in 0.1 M KCl solution under a scanning electrical potential from −2 to +2 V. The *I*−*V* curves were recorded before and after modification with ferroporphyrin in the absence and presence of NO, respectively. As illustrated in Figure 3a, the unmodified PET film shows a nonlinear curve: the ion current is ca. −188.0 nA at −2 V, ca. 62.5 nA at +2 V, giving a rectification ratio of 3.0 (Figure 3b, black column). The rectification ratio was calculated by the absolute values of ion current at a given voltage −2 V versus 2 V. After modification with ferroporphyrin, the ion current declined dramatically to −15.8 nA at −2 V and 23.2 nA at +2 V. The ion current rectification vanished (Figure 3b, wine column). Significant variation is attributed to the surface charge disappearance. During the modification process, the steric hindrance between ferroporphyrin molecules makes the coupled reaction incomplete, and excess carboxyl acid groups remain. The residual carboxyl acid groups can coordinate to ferroporphyrin, which transforms the negative surface to the close-to-neutral state, preventing the ions transport. Interestingly, NO can be used to open the nanochannels. After bubbling NO to the ferroporphyrin blocked nanochannels, the ion current increases sharply to −126.9 nA at −2.0 V (Figure 3a, violet line), and the diode-like behavior appears again. However, the *I*−*V* curve of the unmodified nanochannels appears to experience no change in the presence of NO (Figure S6), which indicates that NO cannot change the surface charges of the unmodified ones. Besides, the rectification ratio reaches 14.52 after bubbling NO (Figure 3b, violet column). This is because NO can coordinate to ferroporphyrin preferentially and release the carboxyl acid groups. The surfaces of the nanochannels became negatively charged, and cations pass preferentially from the tip to the base of the nanochannels due to the asymmetric conical shape (Figure S7), while anions are rejected, which show their ionic transport preference in one direction. Thereby, the ion current rectification recovered. Just like the ion channels in nature, these artificial ion nanochannels are activated though the coordination of NO and ferroporphyrin. The surface changes of the nanochannels can also be reflected by gating ratio, which

DOI: 10.1021/acsami.7b14505
ACS Appl. Mater. Interfaces 2018, 10, 3241−3247

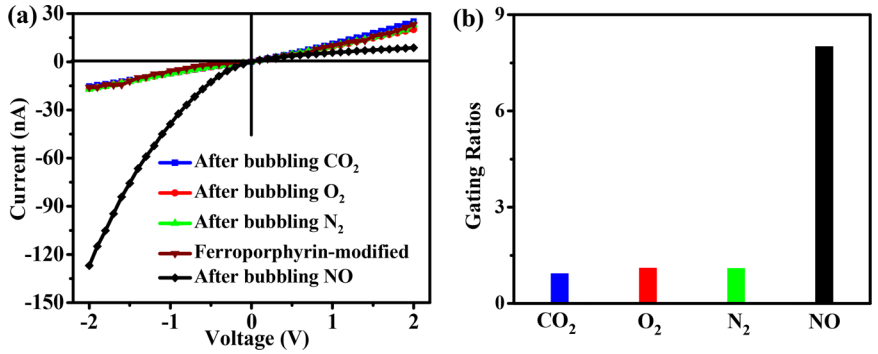

Figure 5. (a) Selectivity of the nanofluidic sensing system in 0.1 M KCl solution: $I-V$ curves of the modified nanochannels by bubbling CO_2, O_2, N_2, and NO, respectively. (b) Gating ratios of the modified nanochannels in the presence of CO_2, O_2, N_2, and NO, respectively.

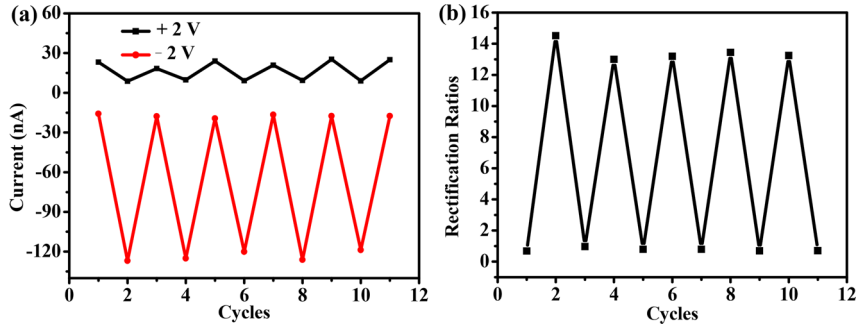

Figure 6. (a) Ion current transition of ion nanochannels at +2 and −2 V with NO bubbling and pulse laser illumination, showing excellent reproducibility and stability. (b) Changes between the two states of rectification ratios.

was defined as I_{ON}/I_{OFF}, (where I_{ON} and I_{OFF} are the currents measured at −2 V after and before NO ventilation, respectively). As shown in Figure 3c, the ion gating ratio of the nanofluidic sensing system reaches up to 8, higher than that of the unmodified nanochannels.

To investigate the response rate of this NO-sensing system, we recorded the ion currents with different NO ventilation time. As shown in Figure 4a, after bubbling NO into the ferroporphyrin-blocked nanochannels for only 4s, obvious nonlinear $I-V$ curve can be observed. As NO was continuously ventilated, the ion current (Figure 4a) and rectification ratio (Figure 4b) increased correspondingly, which indicated that the nanochannels turned on gradually. In the initial stage, only parts of carboxyl acid groups were released by NO. The longer NO ventilation time results in more released carboxyl acid groups, which contributes to a dramatic current increase. The nanochannels can be opened within 10 s. The current value and rectification ratios are comparable to those of 60 s. The fast responsive rate is necessary in living creatures so that they can quickly respond to external stimuli.

Because NO exhibits a higher binding affinity to ferroporphyrin, we examined the selectivity of this ferroporphyrin-modified nanochannels for NO in comparison with other gases. As shown in Figure 5a, the system exhibits excellent selectivity for NO. When the nanofluidic sensing system was treated with CO_2, O_2, and N_2, no obvious diode-like behavior can be observed, and the corresponding gating ratios were all approximately 1 (Figure 5b). However, the nanogating turns on with the rectification of the $I-V$ curve after treatment with NO. The reason is that only the highly reactive NO can coordinate to the ferroporphyrin effectively, releasing the carboxyl acid groups. In our previous study, we found that CO could also bind to ferroporphyrin. CO recovered the ferroporphyrin-blocked nanochannels.[39] However, the bonding strength between NO and ferroporphyrin is much bigger. The equilibrium constant of NO binding to ferroporphyrin is 1500-fold larger than that of CO.[40] Thus, NO can release far more carboxyl acid groups than CO. Compared with our previous work related to CO,[39] this NO-sensing system gives a higher rectification ratio and gating ratio. This result is consistent with many biologically important processes in creatures in which NO operates, rather than CO. It is the high reactivity that makes NO special. Therefore, this NO-activated nanofluidic diode can be applied in the fields of NO detection.

Furthermore, this NO-sensing system can be regulated by light. Nitrosyl adducts of metalloporphyrins are known to be light sensitive, losing NO after exposure to visible light.[38] Before bubbling NO, the ferroporphyrin blocked nanochannels were in an OFF-state with low current. After activation with NO, the carboxyl acid groups were released. The nanochannels turned to the ON-state. Followed with exposure the ferroporphyrin-modified nanochannel to 532 nm pulse laser in ferroporphyrin solution for 30 min, most of the NO was released. Meanwhile, ferroporphyrin coordinate to carboxyl acid groups, making the surface of the channel close-to-neutral. Consequently, the channels returned to the OFF-state. Figure 6a shows the ON/OFF switch upon alternating addition and removal of NO. After several cycles, no obvious ion current damping was observed. Similar results for the rectification switching are presented in Figure 6b. Both results show excellent reversibility and stability of this system. This light regulated NO-sensing system provides a new way for the delivery of NO.

Ionic transport properties of the nanofluidic sensing system have also been investigated by different concentrations of KCl solution (Figure 7a and Table S1). As the concentration of KCl

DOI: 10.1021/acsami.7b14505
ACS Appl. Mater. Interfaces 2018, 10, 3241−3247

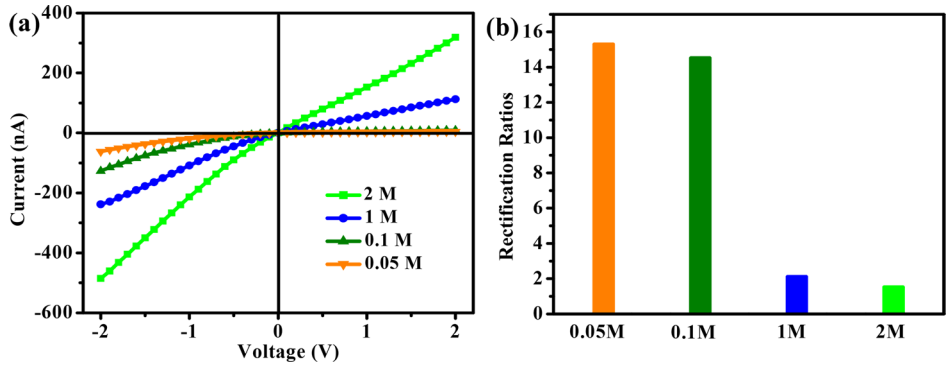

Figure 7. *I*–*V* curves of the nanofluidic sensing system in KCl electrolyte with different concentrations (a), and the corresponding ion rectification ratios (b).

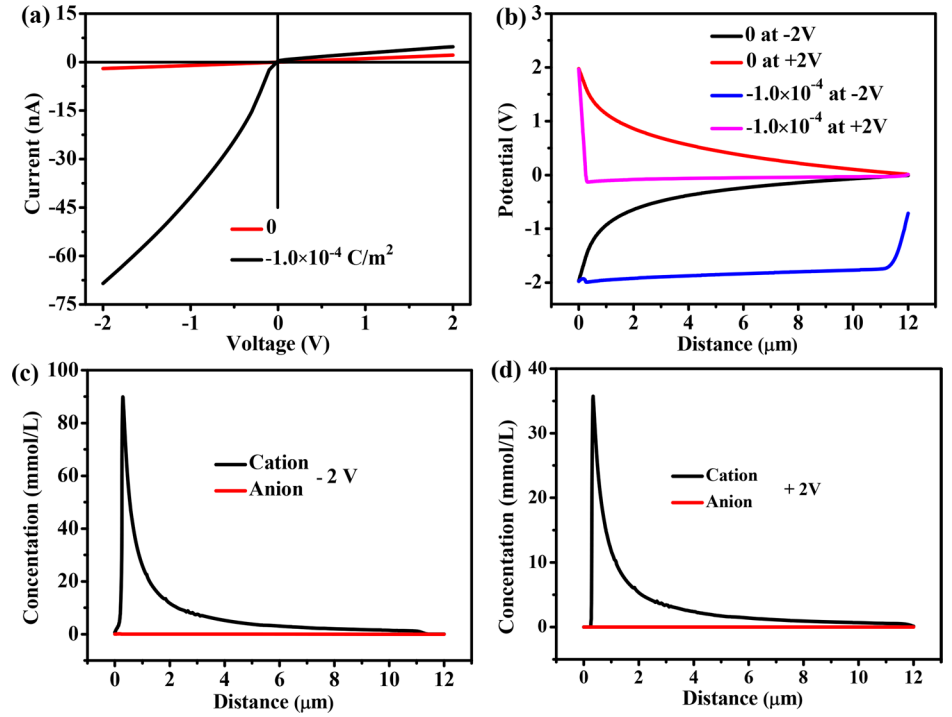

Figure 8. (a) Simulated *I*–*V* curves of the nanochannels before and after NO ventilation. (Before ventilation, the surface charge is considered to be zero; after ventilation, the surface charge is defined as -1×10^{-4} C m^{-2}.) The simulated results are consistent with the experimental results based on the Poisson and Nernst–Planck equations. (b) Potential distributions in the nanochannels when the applied external voltage is −2 and +2 V in the presence and absence of NO. (c) Cation concentration distribution along the nanochannel at −2 V after NO ventilation. (d) Cation concentration distribution along the nanochannel at +2 V after NO ventilation.

increases, the ion current increases dramatically. It should be noted that the ion current rectification behavior is significantly sensitive to the concentrations of electrolyte. As displayed in Figure 7b, higher rectification ratios were achieved in lower concentrations of electrolyte solution. For 0.05 M of KCl solution, the ion rectification ratio is 15.3. However, the ion current rectification behavior of the nanofluidic sensing system dies down as the electrolyte concentration increase. When the concentration of KCl electrolyte is 2M, the rectification ratio is only 1.5. Extensive research has confirmed that the ion rectification phenomenon relies on the electric double layer and surface charge density of nanopores or nanochannels.[41,42] Normally, the electric double layer can overlap the nanochannels well in lower concentrations of electrolyte and the ion transport across the nanochannels is controlled by the surface charge, which contributes to evident ion rectification behavior. Nevertheless, the electric double layer is attenuated with the increase of electrolyte concentration. Therefore, no obvious ion rectification behavior could be observed in high concentration KCl solutions.[43,44]

In order to quantitatively investigate the ion rectification properties of this nanochannel system, a theoretical simulation based on Poisson and Nernst–Plank (PNP) model was established. The Nernst–Planck equation which describes the transport behavior of charged nanochannels is as follows:

$$J_i = -D_i(\nabla C_i + Z_i C_i \nabla \varphi) + C_i V_{eof}, \quad i = +, -$$

(i = + stands for cations, and i = − stands for anions) together with the steady-state continuity equation and the Poisson equation,

$$\nabla J_i = 0, \quad i = +, -$$

DOI: 10.1021/acsami.7b14505
ACS Appl. Mater. Interfaces 2018, 10, 3241–3247

$$\nabla^2\varphi = \frac{F^2}{\varepsilon RT}(C_- - C_+)$$

where J_i, D_i, Z_i, and C_i is the flux of ions, diffusion coefficient, charge number, and ion concentration for each ionic species i. φ denotes the local dimensionless electric potential, and V_{eof} is electroosmotic velocity. The software COMSOL Multiphysics was used to simulate the ion rectification process of the conical nanochannel. The boundary conditions in this model are shown below: the electrolyte solution concentration is $c_L = c_R = 0.1$ mol L^{-1} in this work; the model is along the center axis of nanochannel; the thickness of membrane in the simulated models is set as 12 μm; and the diffusion coefficients of anion and cation are set as 1.93×10^{-5} and 2.03×10^{-5} cm^2 s^{-1}.

Figure 8a displays the simulated $I-V$ curves. Clearly, the nanochannels rectify the ion current after the ventilation of NO. The rectification ratio reaches 14.46, which is comparable to the 14.52 achieved in our experiment. After light exposure, the ion rectification disappeared. Figure 8b presents the electric potential distribution inside the nanochannel before and after bubbling NO at +2 and −2 V, respectively. Before bubbling NO, the electric potential distribution is symmetrical at +2 V and −2 V. After bubbling NO, the symmetrical electric potential distribution was broken, due to the asymmetry charge distribution, which contributes to a higher rectification ratio. At −2 V, cations are driven to the base side, and anions are driven to the tip side. With the negative surface charge, cations were attracted while anions were rejected at the tip region. The ion current and ion conductance increase. At + 2 V, the situation is quite opposite. Cations were driven to the tip region, and the ion current and ion conductance decrease. Consequently, the ion current is asymmetric, and this system rectifies the ion current, which is consistent with our experimental result.

Figure 8c,d presents the theoretical ion concentration distribution profiles along the central axis inside the nanochannels at positive (+2 V) and negative (−2 V) bias. They indicate that the concentration of cations is much higher than that of anions at the tip side under both bias. After bubbling with NO, the nanochannel surface became negatively charged. According to the parameters and assumption of boundary conditions set, the surface charge density is defined as -1.0×10^{-4} C/m^2. As the tip zone has a radius comparable to the electric double layer, it contributes to the higher conductance and accumulation of opposite charged ions. Therefore, the cations are much more abundant than anions at the tip side. Besides, the applied voltage can also control the movement of ions. Apparently, the cations assemble to a higher degree at −2 V than at +2 V. Therefore, the conical nanochannel and the negatively charged nanochannel wall contribute to the asymmetric distribution of ions near the surface. This simulation well supported the NO induced ion current rectification behavior in the nanochannels.

4. CONCLUSIONS

We have successfully designed an NO and light cooperative nanofluidic diode inspired by the NO-activated ion channels in guard cells. The nanofluidic devices were constructed by functionalizing with ferroporphyrin via coupled reaction in porous PET membrane. The nanochannels turn on when the highly reactive NO binds to ferroporphyrin. After visible light exposure, NO dissociates from the nitrosyl ferroporphyrin, resulting in the OFF-state. Furthermore, the nanofluidic sensing system exhibits characteristics of excellent reversibility and stability. The conclusive simulation results, which employ the PNP model, are highly consistent with the experimental results. These results help us better understand biological responsive behaviors in nature. Furthermore, potential application may be in gas detection and remote control of mass delivery.

■ ASSOCIATED CONTENT

Supporting Information

The Supporting Information is available free of charge on the ACS Publications website at DOI: 10.1021/acsami.7b14505.

XPS spectrum of PET film before and after ferroporphyrin modification. $I-V$ curves of the unmodified nanochannels in the presence and absence of NO. Current measurements of the nanofluidic sensing system at different concentrations of KCl solutions (PDF)

■ AUTHOR INFORMATION

Corresponding Authors

*E-mail: zhaijin@buaa.edu.cn (J.Z.).
*E-mail: lcgao@buaa.edu.cn (L.G.).

ORCID

Jin Zhai: 0000-0003-3596-411X

Notes

The authors declare no competing financial interest.

■ ACKNOWLEDGMENTS

This work was supported by the National Key Research and Development Program of China (2017YFA0206902, 2017YFA0206900), and the National Natural Science Foundation (21641006).

■ REFERENCES

(1) Beckman, J. S.; Koppenol, W. H. Nitric oxide, Superoxide, and Peroxynitrite: the Good, the Bad, and Ugly. *Am. J. Physiol Cell Physiol* **1996**, *271*, C1424−C1437.

(2) Delledonne, M.; Xia, Y. J.; Dixon, R. A.; Lamb, C. Nitric Oxide Functions as a Signal in Plant Disease Resistance. *Nature* **1998**, *394*, 585−588.

(3) Guo, F. Q.; Okamoto, M.; Crawford, N. M. Identification of a Plant Nitric Oxide Synthase Gene Involved in Hormonal Signaling. *Science* **2003**, *302*, 100−103.

(4) Rockel, P.; Strube, F.; Rockel, A.; Wildt, J.; Kaiser, W. M. Regulation of Nitric Oxide (NO) Production by Plant Nitrate Reductase in Vivo and in Vitro. *J. Exp. Bot.* **2002**, *53*, 103−110.

(5) Lamattina, L.; García-Mata, C.; Graziano, M.; Pagnussat, G. Nitric Oxide: the Versatility of an Extensive Signal Molecule. *Annu. Rev. Plant Biol.* **2003**, *54*, 109−136.

(6) Delledonne, M.; Zeier, J.; Lamb, C.; Marocco, A. Signal Interactions between Nitric Oxide and Reactive Oxygen Intermediates in the Plant Hypersensitive Disease Resistance Response. *Proc. Natl. Acad. Sci. U. S. A.* **2001**, *98*, 13454−13459.

(7) Durner, J.; Klessig, D. F. Nitric Oxide as a Signal in Plants. *Curr. Opin. Plant Biol.* **1999**, *2*, 369−374.

(8) Sokolovski, S.; Blatt, M. R. Nitric Oxide Block of Outward-rectifying K^+ Channels Indicates Direct Control by Protein Nitrosylation in Guard Cells. *Plant Physiol.* **2004**, *136*, 4275−4284.

(9) Renganathan, M.; Cummins, T. R.; Waxman, S. G. Nitric Oxide Blocks Fast, Slow, and Persistent Na^+ Channels in C-type DRG Neurons by S-nitrosylation. *J. Neurophysiol.* **2002**, *87*, 761−775.

(10) Garcia-Mata, C.; Gay, R.; Sokolovski, S.; Hills, A.; Lamattina, L.; Blatt, M. R. Nitric Oxide Regulates K^+ and Cl^- Channels in Guard Cells through a Subset of Abscisic Acid-evoked Signaling Pathways. *Proc. Natl. Acad. Sci. U. S. A.* **2003**, *100*, 11116−11121.

DOI: 10.1021/acsami.7b14505
ACS Appl. Mater. Interfaces 2018, 10, 3241−3247

(11) Traylor, T. G.; Sharma, V. S. Why NO? *Biochemistry* **1992**, *31*, 2847−2849.
(12) Gayatri, G.; Agurla, S.; Raghavendra, A. S. Nitric Oxide in Guard Cells as an Important Secondary Messenger during Stomatal Closure. *Front. Plant Sci.* **2013**, *4*, 1−11.
(13) Hosy, E.; Vavasseur, A.; Mouline, K.; Dreyer, I.; Gaymard, F.; Porée, F.; Boucherez, J.; Lebaudy, A.; Bouchez, D.; Very, A. A.; Simonneau, T.; Thibaud, J. B.; Sentenac, H. The Arabidopsis Outward K^+ Channel GORK is Involved in Regulation of Stomatal Movements and Plant Transpiration. *Proc. Natl. Acad. Sci. U. S. A.* **2003**, *100*, 5549−5554.
(14) Shang, X. M.; Xie, G. H.; Kong, X. Y.; Zhang, Z.; Zhang, Y. Q.; Tian, W.; Wen, L. P.; Jiang, L. An Artificial CO_2-driven Ionic Gate Inspired by Olfactory Sensory Neurons in Mosquitoes. *Adv. Mater.* **2017**, *29*, 1603884.
(15) Sui, X.; Zhang, Z.; Zhang, Z. Y.; Wang, Z. W.; Li, C.; Yuan, H.; Gao, L. C.; Wen, L. P.; Fan, X.; Yang, L. J.; Zhang, X. R.; Jiang, L. Biomimetic Nanofluidic Diode Composed of Dual Amphoteric Channels Maintains Rectification Direction over a Wide pH Range. *Angew. Chem., Int. Ed.* **2016**, *55*, 13056−13060.
(16) Hou, X.; Zhang, H. C.; Jiang, L. Building Bio-Inspired Artificial Functional Nanochannels: From Symmetric to Asymmetric Modification. *Angew. Chem., Int. Ed.* **2012**, *51*, 5296−5307.
(17) Zhang, H. C.; Hou, X.; Hou, J.; Zeng, L.; Tian, Y.; Li, L.; Jiang, L. Synthetic Asymmetric-Shaped Nanodevices with Symmetric pH-Gating Characteristics. *Adv. Funct. Mater.* **2015**, *25*, 1102−1110.
(18) Hou, X.; Liu, Y. J.; Dong, H.; Yang, F.; Li, L.; Jiang, L. A pH-Gating Ionic Transport Nanodevice: Asymmetric Chemical Modification of Single Nanochannels. *Adv. Mater.* **2010**, *22*, 2440−2443.
(19) Meng, Z. Y.; Chen, Y.; Li, X. L.; Xu, Y. L.; Zhai, J. Cooperative Effect of pH-Dependent Ion Transport within Two Symmetric-Structured Nanochannels. *ACS Appl. Mater. Interfaces* **2015**, *7*, 7709−7716.
(20) Ali, M.; Ramirez, P.; Mafé, S.; Neumann, R.; Ensinger, W. A pH-tunable Nanofluidic Diode with a Broad Range of Rectifying Properties. *ACS Nano* **2009**, *3*, 603−608.
(21) Buchsbaum, S. F.; Nguyen, G.; Howorka, S.; Siwy, Z. S. DNA-modified Polymer Pores Allow pH-and Voltage-gated Control of Channel Flux. *J. Am. Chem. Soc.* **2014**, *136*, 9902−9905.
(22) Koçer, A.; Walko, M.; Meijberg, W.; Feringa, B. L. A Light-Actuated Nanovalve Derived from a Channel Protein. *Science* **2005**, *309*, 755−758.
(23) Sun, Y.; Ma, J. K.; Zhang, F.; Zhu, F.; Mei, Y. X.; Liu, L.; Tian, D. M.; Li, H. B. A Light-Regulated Host-Guest-based Nanochannel System Inspired by Channelrhodopsins Protein. *Nat. Commun.* **2017**, *8*, 260.
(24) Li, P.; Xie, G. H.; Kong, X. Y.; Zhang, Z.; Xiao, K.; Wen, L. P.; Jiang, L. Light-controlled Ion Transport Through Biomimetic DNA-based Channels. *Angew. Chem., Int. Ed.* **2016**, *55*, 15637−15641.
(25) Xie, X. J.; Crespo, G. A.; Mistlberger, G.; Bakker, E. Photocurrent Generation Based on a Light-driven Proton Pump in an Artificial Liquid Membrane. *Nat. Chem.* **2014**, *6*, 202−207.
(26) Hou, X. Smart Gating Multi-Scale Pore/Channel-Based Membranes. *Adv. Mater.* **2016**, *28*, 7049−7064.
(27) Hou, X.; Jiang, L. Learning from Nature: Building Bio-Inspired Smart Nanochannels. *ACS Nano* **2009**, *3*, 3339−3342.
(28) Yameen, B.; Ali, M.; Neumann, R.; Ensinger, W.; Knoll, W.; Azzaroni, O. Ionic Transport through Single Solid-state Nanopores Controlled with Thermally Nanoactuated Macromolecular Gates. *Small* **2009**, *5*, 1287−1291.
(29) Chen, Y.; Zhou, D.; Meng, Z. Y.; Zhai, J. An Ion-gating Multinanochannel System Based on a Copper-responsive Self-cleaving DNAzyme. *Chem. Commun.* **2016**, *52*, 10020−10023.
(30) Hou, X.; Guo, W.; Jiang, L. Biomimetic smart nanopores and nanochannels. *Chem. Soc. Rev.* **2011**, *40*, 2385−2401.
(31) Braha, O.; Gu, L. Q.; Zhou, L.; Lu, X. F.; Cheley, S.; Bayley, H. Simultaneous Stochastic Sensing of Divalent Metal Ions. *Nat. Biotechnol.* **2000**, *18*, 1005−1007.
(32) Hou, X.; Guo, W.; Xia, F.; Nie, F. Q.; Dong, H.; Tian, Y.; Wen, L. P.; Wang, L.; Cao, L. X.; Yang, Y.; Xue, J. M.; Song, Y. L.; Wang, Y. G.; Liu, D. S.; Jiang, L. A Biomimetic Potassium Responsive Nanochannel: G-quadruplex DNA Conformational Switching in a Synthetic Nanopore. *J. Am. Chem. Soc.* **2009**, *131*, 7800−7805.
(33) Harrell, C. C.; Kohli, P.; Siwy, Z.; Martin, C. R. DNA-nanotube Artificial ion Channels. *J. Am. Chem. Soc.* **2004**, *126*, 15646−15647.
(34) Lan, W. J.; Holden, D. A.; White, H. S. Pressure-dependent Ion Current Rectification in Conical-shaped Glass Nanopores. *J. Am. Chem. Soc.* **2011**, *133*, 13300−13303.
(35) Kong, Y.; Fan, X.; Zhang, M. H.; Hou, X.; Liu, Z. Y.; Zhai, J.; Jiang, L. Nanofluidic Diode Based on Branched Alumina Nanochannels with Tunable Ionic Rectification. *ACS Appl. Mater. Interfaces* **2013**, *5*, 7931−7936.
(36) Ishibashi, Y.; Duncker, D. J.; Zhang, J. Y.; Bache, R. J. ATP-sensitive K^+ Channels, Sdenosine, and Nitric Oxide−mediated Mechanisms Account for Coronary Vasodilation during Exercise. *Circ. Res.* **1998**, *82*, 346−359.
(37) Ford, P. C.; Lorkovic, I. M. Mechanistic Aspects of the Reactions of Nitric Oxide with Transition-metal Complexes. *Chem. Rev.* **2002**, *102*, 993−1018.
(38) Hoshino, M.; Kogure, M. Photochemistry of Nitrosyl Porphyrins in the Temperature Range 180−300 K and the Effects of Pyridlne on Photodenitrosylation of Nitrosyliron Tetraphenylporphyrln. *J. Phys. Chem.* **1989**, *93*, 5478−5484.
(39) Xu, Y. L.; Sui, X.; Jiang, J. Q.; Zhai, J.; Gao, L. C. Smooth Muscle Cell-Mimetic CO-regulated Ion Nanochannels. *Adv. Mater.* **2016**, *28*, 10780−10785.
(40) Bohle, D. S.; Hung, C. H. Ligand-Promoted Rapid Nitric Oxide Dissociation from Ferrous Porphyrin Nitrosyls. *J. Am. Chem. Soc.* **1995**, *117*, 9584−9585.
(41) Zhang, H. C.; Hou, X.; Yang, Z.; Yan, D. D.; Li, L.; Tian, Y.; Wang, H. T.; Jiang, L. Bio-inspired Smart Single Asymmetric Hourglass Nanochannels for Continuous Shape and Ion Transport Control. *Small* **2015**, *11*, 786−791.
(42) Jiang, Z. Y.; Liu, H. L.; Ahmed, S. A.; Hanif, S.; Ren, S. B.; Xu, J. J.; Chen, H. Y.; Xia, X. H.; Wang, K. Insight into Ion Transfer through the Sub-nanometer Channels in Zeolitic Imidazolate Frameworks. *Angew. Chem., Int. Ed.* **2017**, *56*, 4767−4771.
(43) Zhang, H. C.; Tian, Y.; Hou, J.; Hou, X.; Hou, G. L.; Ou, R. W.; Wang, H. T.; Jiang, L. Bioinspired Smart Gate-Location-Controllable Single Nanochannels: Experiment and Theoretical Simulation. *ACS Nano* **2015**, *9*, 12264−12273.
(44) Zhang, Q. Q.; Liu, Z. Y.; Wang, K. F.; Zhai, J. Organic/inorganic Hybrid Nanochannels Based on Polypyrrole-embedded Alumina Nanopore Arrays: pH- and Light-Modulated Ion Transport. *Adv. Funct. Mater.* **2015**, *25*, 2091−2098.

DOI: 10.1021/acsami.7b14505
ACS Appl. Mater. Interfaces 2018, 10, 3241−3247